Ceramics International xxx (xxxx) xxx–xxx

Contents lists available at ScienceDirect

Ceramics International

journal homepage: www.elsevier.com/locate/ceramint

$Li_4Mg_3Ti_2O_9$: A novel low-loss microwave dielectric ceramic for LTCC applications

Jinxin Bi, Yunjuan Niu, Haitao Wu*

School of Materials Science and Engineering, University of Jinan, Jinan 250022, China

ARTICLE INFO

Keywords:
$Li_4Mg_3Ti_2O_9$
Microwave dielectric properties
Infrared spectroscopy
LTCC

ABSTRACT

Low-loss novel $Li_4Mg_3Ti_2O_9$ dielectric ceramics with rock-salt structure were prepared by a conventional solid-state route. The crystalline structure, chemical bond properties, infrared spectroscopy and microwave dielectric properties of the abovementioned system were initially investigated. It could be concluded from this work that the extrinsic factors such as sintering temperatures and grain sizes significantly affected the dielectric properties of $Li_4Mg_3Ti_2O_9$ at lower sintering temperatures, while the intrinsic factors like bond ionicity and lattice energy played a dominant role when the ceramics were densified at 1450 °C. In order to explore the origin of intrinsic characteristics, complex dielectric constants (ε' and ε'') were calculated by the infrared spectra, which indicated that the absorptions of phonon oscillation predominantly effected the polarization of the ceramics. The $Li_4Mg_3Ti_2O_9$ ceramics sintered at 1450 °C exhibited excellent properties of ε_r=15.97, $Q{\cdot}f$=135,800 GHz and τ_f=−7.06 ppm/°C. In addition, certain amounts of lithium fluoride (LiF) were added to lower the sintering temperatures of matrix. The $Li_4Mg_3Ti_2O_9$–3 wt% LiF ceramics sintered at 900 °C possessed suitable dielectric properties of ε_r=15.17, $Q{\cdot}f$ =42,800 GHz and τ_f=−11.30 ppm/°C, which made such materials promising for low temperature co-fired ceramic applications (LTCC).

1. Introduction

With the rapid development of mobile communication, microwave dielectric ceramics have attracted more and more attentions due to their remarkable advantages in microwave devices such as dielectric resonators, antennas, microwave filters and so on [1,2]. These materials are basically required to possess an appropriate dielectric constant to reduce devices sizes, a high quality factor for frequency selectivity and a near-zero temperature coefficient of resonant frequency for temperature stability [3,4]. Moreover, in order to meet the requirements of miniaturization and integration, the ceramics should also be sintered below 960 °C for being co-fired with Ag electrode (LTCC) [5,6].

Recently, the Li_2O-MgO-TiO_2 ceramics have been extensively investigated due to their excellent microwave dielectric properties and potential applications in LTCC [7–18]. For example, Sebastian et al. reported that the cubic spinel $Li_2MgTi_3O_8$ ceramics showed the dielectric property of ε_r=27.2, $Q{\cdot}f$=42,000 GHz and τ_f=3.2 ppm/°C [7]. The densified $Li_2Mg_3Ti_4O_{12}$ ceramics, which belonged to a space group of Fd-3m, could be obtained at 1125 °C with ε_r=20.2, $Q{\cdot}f$=62,300 GHz and τ_f=−27.1 ppm/°C [8]. A pseudo phase diagram of Li_2O-MgO-TiO_2 ternary system was firstly established by Zhou et al. on the basis of various data reported in previous works [9], which indicated that the phase compositions and dielectric properties of ceramics were significantly affected by the ratio of Li:Mg:Ti. More specifically, there were a great number of reports about the rock-salt structured Li_2O-MgO-TiO_2 compounds owing to their higher $Q{\cdot}f$ values [11–16]. According to the partial subsolidus phase diagram of Li_2TiO_3-MgO, monoclinic structured Li_2TiO_3 might be transformed into cubic rock salt phase when MgO content was beyond 40 mol% [10]. The structural evolution in the above system was also confirmed by Bian et al.. In their report, the $0.6Li_2TiO_3$+0.4MgO ceramics sintered at 1350 °C possessed dielectric properties of ε_r=17.25, $Q{\cdot}f$=97,300 GHz and τ_f=~−25 ppm/°C with a space group of Fm-3m [11]. A higher $Q{\cdot}f$ value of 152,000 GHz could be obtained by rock-salt structured $Li_2Mg_3TiO_6$ ($0.75Li_2TiO_3$+0.25MgO) ceramics with ε_r=15.2 and τ_f=−39 ppm/°C [12]. Huang et al. investigated that the Li_2MgTiO_4 ($0.5Li_2TiO_3$+0.5MgO) ceramics possessed the properties of ε_r=18, $Q{\cdot}f$=90,000 GHz and τ_f=−27.2 ppm/°C at a lower sintering temperature (1350 °C) [13]. In addition, Zhou et al. investigated that the adjustable dielectric properties could be achieved by using a series of $Mg_{1-x}Li_{2x}Ti_xO_{1+2x}$ ($Li_2Mg_4TiO_7$, $Li_2Mg_3TiO_6$, $Li_2Mg_2TiO_5$ and Li_2MgTiO_4) solid solutions [14]. However, the evaporation of lithium seriously affected the densification and structure-property relationship

* Corresponding author.
E-mail address: mse_wuht@ujn.edu.cn (H. Wu).

http://dx.doi.org/10.1016/j.ceramint.2017.03.041
Received 3 February 2017; Received in revised form 1 March 2017; Accepted 6 March 2017

of samples in all the above-mentioned reports. In our previous works, the Li_2MgTiO_4 and $Li_2Mg_3TiO_6$ compounds were synthesized by the atmosphere-protective sintering method to suppress lithium evaporation. The former possessed a higher dielectric constant (15.07) and a near-zero τ_f value (−3.81 ppm/°C), while the latter exhibited an excellent $Q{\cdot}f$ value of 153,000 GHz [15,16].

Based on the above results, the $Li_4Mg_3Ti_2O_9$ ceramics, which could be divided into $0.4Li_2TiO_3$+0.6MgO, were chosen as a candidate for optimizing a balanced property in Li_2O-MgO-TiO_2 system. However, there were insufficient data to predict the crystal structure and dielectric properties of these ceramics. Hence, the rock-salt structured $Li_4Mg_3Ti_2O_9$ ceramics were synthesized via the solid state method in this work. The relationships among phase composition, microstructure, sintering characteristics, infrared spectra and microwave dielectric properties of the system were systematically investigated. Complex chemical bond theory was used to characterize the bond ionicity and lattice energy of individual bonds. In addition, the lithium fluoride (LiF) was used as sintering aids to decrease the sintering temperature of the matrix. The sintering behaviors as well as dielectric properties of $Li_4Mg_3Ti_2O_9$-xwt%LiF compounds were studied in the present work.

2. Experimental procedure

The $Li_4Mg_3Ti_2O_9$ ceramics were prepared via the conventional solid-state route. High purity Li_2CO_3, MgO and TiO_2 (99.99%, Aladdin Shanghai Biochemical Technology Co., Ltd. Shanghai, China) were weighted according to the stoichiometric formulation of $Li_4Mg_3Ti_2O_9$. The starting powders were mixed with anhydrous ethanol for 24 h in a nylon container, dried and calcined at 1050 °C for 2 h in the alumina crucibles. After subsequent ball-milling with 0–5 wt% lithium fluoride, the resultant powders were mixed with 8 wt% polyvinyl alcohol, granulated and pressed into cylindrical disks of 10 mm diameter and about 6 mm height at a pressure of about 200 MPa. All the obtained pellets were preheated at 500 °C for 4 h to expel the organic binder. In order to suppress the lithium evaporation, the matrix were covered with sacrificial powders and sintered at 1300–1450 °C for 4 h in platinum crucibles at a heating rate of 5 °C/min, while the LiF-doped $Li_4Mg_3Ti_2O_9$ samples were sintered at 700–1200 °C in air.

Phase analysis of samples was conducted with the help of a Rigaku diffractometer using Ni filtered CuKα radiation (λ=0.1542 nm) at 40 kV and 40 mA settings. The microstructures of $Li_4Mg_3Ti_2O_9$ were examined using a scanning electron microscope (Model JEOL JEM-2010, FEI Co., Japan) coupled with energy dispersive X-ray spectroscopy (EDS). The apparent densities of sintered samples were measured using the Archimedes method (Mettler ToledoXS64). Infrared reflectivity spectra were measured using a Bruker IFS 66v FTIR spectrometer on Infrared beamline station (U4) at National Synchrotron Radiation Lab. (NSRL) in China. A network analyzer was used for the measurement of microwave dielectric properties. Dielectric constants were measured using Hakki-Coleman post-resonator method by exciting the TE011 resonant mode of dielectric resonator by using an electric probe as suggested by Hakki and Coleman [19]. Unloaded quality factors were measured using TE01d mode by the cavity method [20]. All measurements were finished at room temperature and in the frequency of 8–12 GHz. The temperature coefficients of the resonant frequency (τ_f) were calculated from the data collected in the temperature range of 25–85 °C according to $\tau_f=\Delta f/(f_0\Delta T)$, where f_0 was the frequency at 25 °C.

3. Results and discussion

Fig. 1 showed the variation of diametric shrinkage ratio and apparent densities with sintering temperature for $Li_4Mg_3Ti_2O_9$ samples. As the sintering temperature increasing from 1350 to 1425 °C, the apparent density gradually increased from 2.92 to 3.15 g/cm^3. After

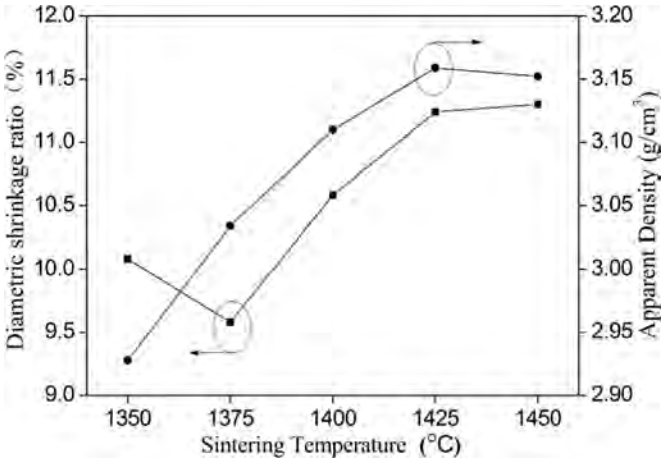

Fig. 1. Apparent densities and shrinkage ratio of $Li_4Mg_3Ti_2O_9$ ceramics as a function of sintering temperatures from 1350 to 1450 °C.

that, the values stabilized at 3.15 g/cm^3 in the temperature region of 1425–1450 °C. The variation of shrinkage ratio showed a similar tendency that the values increased from 9.58% to 10.5% with temperature increasing from 1350 to 1450 °C. The SEM micrographs of $Li_4Mg_3Ti_2O_9$ samples obtained at various sintering temperatures were illustrated in Fig. 2(a-e). The microstructure with small pores could be observed when the samples were sintered at 1350 °C. By contrast, grain growth of samples with closely-packed grains and discernable grain boundaries was recognized when the sintering temperature increasing from 1375 to 1450 °C, which resulted in the elimination of pores in the matrix. The well-dense sample was comprised of large grains of around 30 μm and small grains of around 10 μm when it was sintered at 1450 °C, which indicated that the evaporation of lithium could be neglected in this work. EDS analysis about grains chosen randomly from specimen sintered at 1450 °C was displayed in Fig. 2(f). The atom ratio of Mg to Ti was approximately to be 3:2, which was corresponded to the theoretical composition of $Li_4Mg_3Ti_2O_9$.

XRD patterns of $Li_4Mg_3Ti_2O_9$ specimens sintered at different temperatures were presented in Fig. 3. All the diffraction peaks could be indexed as the standard pattern of rock-salt structured $LiFeO_2$ (JCPDS #70–2711), which indicated that $Li_4Mg_3Ti_2O_9$ possessed the same structure with Li_2MgTiO_4 and $Li_2Mg_3TiO_6$. There were no significant changes in the angle and intensity of the diffraction peaks, implying the good crystallinity of all the samples. The unit cell volume of $Li_4Mg_3Ti_2O_9$ specimen sintered at 1450 °C was calculated to be V=72.12 Å^3 with a=b=c=4.1626 Å, which was higher than that of Li_2MgTiO_4 (V=71.90 Å^3) and was lower than that of $Li_2Mg_3TiO_6$ (V=73.14 Å^3) reported in our previous works [15,16]. Based on the atomic coordinate information of $LiFeO_2$, the bond length of Li/Mg/Ti-O was calculated to be 2.0816 Å. The schematic crystal structure of rock-salt structured $Li_4Mg_3Ti_2O_9$ was shown in the inset of Fig. 3. It could be observed that three kinds of cations occupied the same atomic positions and were connected with other six oxygen ions, thus the ratio of Li:Mg:Ti would enlarge or compress single Li/Mg/Ti-O octahedral.

In order to initially characterize the structure-property relationship, intrinsic parameters such as lattice energy and bond ionicity were calculated in this work. Based on the crystallographic data reported in our previous works and generalized P-V-L theory reported by Zhang et al., the complex crystal of $Li_4Mg_3Ti_2O_9$ was decomposed as Eq. (1) [21–23].

$$Li_4Mg_3Ti_2O_9 \rightarrow \sum A_mB_n = Li_4O_4 + Mg_3O_3 + Ti_2O_2 \quad (1)$$

Due to the fact that $Li_4Mg_3Ti_2O_9$ had the same crystal structure as Li_2MgTiO_4 and $Li_2Mg_3TiO_6$ compounds, the valence electron numbers and effective valence electron numbers of oxygen anions in every bond could refer to our previous work [15,16]. The bond ionicity of

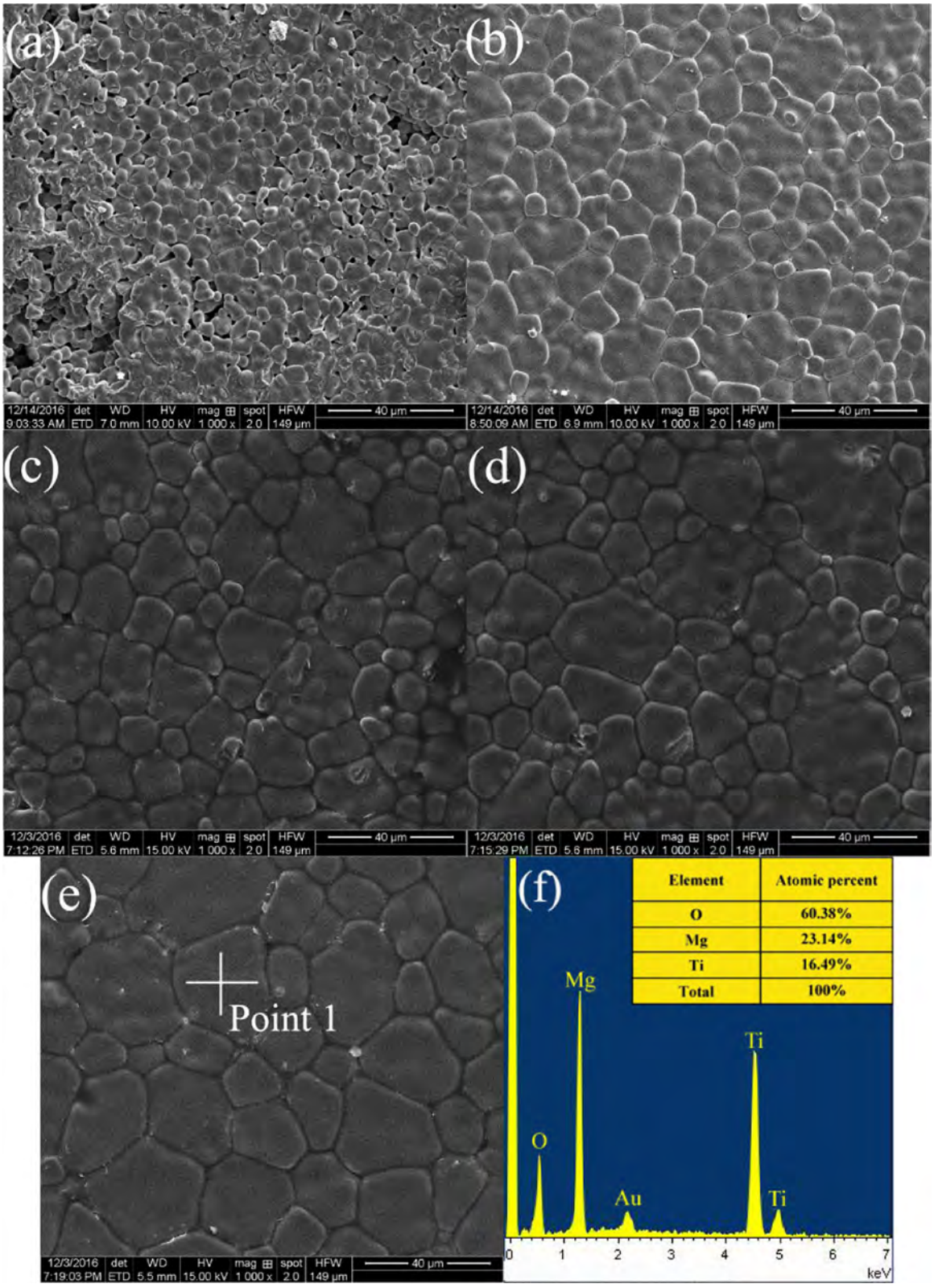

Fig. 2. SEM micrographs of $Li_4Mg_3Ti_2O_9$ ceramics sintered at different temperatures for 4 h (a-e corresponding to 1350 °C, 1375 °C, 1400 °C, 1425 °C and 1450 °C) and (f) EDS analysis about grains chosen randomly from the samples sintered at 1450 °C.

individual bonds was calculated as follows [21–23].

$$f_i^{\mu} = \frac{(C^{\mu})^2}{(E_g^{\mu})^2} \quad (2)$$

$$(E_g^{\mu})^2 = (E_h^{\mu})^2 + (C^{\mu})^2 \quad (3)$$

$$(E_h^{\mu})^2 = \frac{39.74}{(d^{\mu})^{2.48}} \quad (4)$$

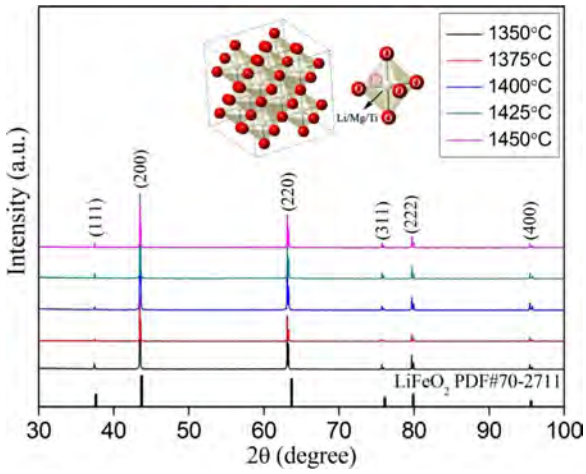

Fig. 3. XRD patterns of $Li_4Mg_3Ti_2O_9$ ceramics sintered at 1350–1450 °C for 4 h and a schematic crystal structure of $Li_4Mg_3Ti_2O_9$.

$$C^{\mu} = 14.4b^{\mu}\exp(-k_s^{\mu}r_0^{\mu})[(Z_A^{\mu})^* - \frac{n}{m}(Z_B^{\mu})^*]/r_0^{\mu} \quad (5)$$

where E_g^{μ} was a combination of homopolar E_h^{μ} and heteropolar C^{μ}, d^{μ} was the bond length of Li/Mg/Ti-O, r_0^{μ}=0.5 d^{μ}, $(Z_A^{\mu})^*$ and $(Z_B^{\mu})^*$ were effective number of valence electrons in ions, b^{μ} was calculated as 3.024 in this work. The Thomas-Fermi screening factor $\exp(-k_s^{\mu}r_0^{\mu})$ was originated from Levine's report [24]. According to the calculated results shown in Table 1 and Fig. 4(a), it was found that the values of f_i were 0.7460, 0.8493, 0.9082 corresponding to the Li-O, Mg-O and Ti-O bond, which indicated that $Li_4Mg_3Ti_2O_9$ was ionic compound with lower covalent bond energy. The dielectric constant was proportional to the bond ionicity, which could be proved in Eq. (6) [25].

$$\varepsilon = \frac{n^2 - 1}{1 - f_i} + 1 \quad (6)$$

where n was a constant of refractive index. Thus, it was considered that the polarizability abilities of $Li_4Mg_3Ti_2O_9$ mainly affected the dielectric constants of the ceramics. In addition, there was a sequence of bond ionicity of f_i (Li-O) < f_i (Mg-O) < f_i (Ti-O), implying that the individual Ti-O bond made a predominant contribution to the dielectric constant.

The lattice energy of crystals could be explained as the energy of crystallization of infinitely-separated ions. It was difficult to characterize the above values by preparing gaseous atoms or ions and measuring the energy change during the crystallization process [26]. However, the lattice energy of $Li_4Mg_3Ti_2O_9$ could be quantitatively calculated using the complex chemical bond theory [21–23]. Based on the results of bond ionicity, the lattice energy of individual bonds could be obtained as follows.

$$U_{cal} = \sum_{\mu} U_b^{\mu} \quad (7)$$

$$U_b^{\mu} = U_{bc}^{\mu} + U_{bi}^{\mu} \quad (8)$$

$$U_{bc}^{\mu} = 2100m\frac{(Z_A^{\mu})^{1.64}}{(d^{\mu})^{0.75}}f_C^{\mu} \quad (9)$$

$$U_{bi}^{\mu} = 1270\frac{(m+n)Z_A^{\mu}Z_B^{\mu}}{d^{\mu}}(1 - \frac{0.4}{d^{\mu}})f_i^{\mu} \quad (10)$$

where U_{bc}^{μ} and U_{bi}^{μ} were covalent and ionic lattice energy of individual bonds. As shown in Table 1, the total lattice energies of individual Li-O, Mg-O and Ti-O bonds were 471, 1864 and 7522 kJ/mol, respectively. The lattice energies ($U_{(A-O)}$) of individual bonds, coupled with molecular lattice energy of $Li_4Mg_3Ti_2O_9$ ceramics were also shown in Fig. 4(b). It was obvious that the lattice energy of Ti-O bond was higher than that of Mg-O and Li-O bond ($U_{(Li-O)} < U_{(Mg-O)} < U_{(Ti-O)}$). What's more, the lattice energy influenced by ionicity was much higher than that influenced by covalence, which indicated that the ionic bonds played a predominant role in affecting the stability of $Li_4Mg_3Ti_2O_9$ crystal.

Microwave dielectric properties of $Li_4Mg_3Ti_2O_9$ ceramics as a function of sintering temperature were shown in Fig. 5. The calculated dielectric properties and measured values were also listed in Table 2. The increased tendency of dielectric constant was the same with that of apparent density at lower sintering temperatures, and a saturated value of 15.97 could be obtained for specimen sintered at 1450 °C. Once the ceramics were sintered well, there were no significant variations of the dielectric constants at higher sintering temperatures. In addition, theoretical dielectric polarizability ($\alpha_{theo.}$) of the samples was calculated by additive rule reported by Shannon et al. [27], while the observed dielectric polarizability ($\alpha_{obs.}$) could be obtained by generalized Clausius-Mossotti equation shown in Eq. (12) [28].

$$\alpha_{theo.} = \alpha(Li_4Mg_3Ti_2O_9) = 4\alpha(Li^+) + 3\alpha(Mg^{2+}) + 2\alpha(Ti^{4+}) + 9\alpha(O^{2-}) \quad (11)$$

$$\alpha_{obs.} = \frac{1}{b}V_m\frac{\varepsilon_r - 1}{\varepsilon_r + 2} \quad (12)$$

where $\alpha(Li^+)$, $\alpha(Mg^{2+})$, $\alpha(Ti^{4+})$, and $\alpha(O^{2-})$ were the ions polarizabilities obtained in Shannon report [27]. In addition, V_m, ε_r and b were the molar volume of $Li_4Mg_3Ti_2O_9$, dielectric constant and a constant ($4\pi/3$). It was noticed that the polarizability of Ti^{4+}(2.93 Å^3) was higher than that of Mg^{2+}(1.32 Å^3) and Li^+(1.20 Å^3), which was corresponding well with the sequence of f_i (Li-O) < f_i (Mg-O) < f_i (Ti-O) calculated in Table 1. By comparison, the values of $\alpha_{theo.}$ (32.17) and $\alpha_{obs.}$(32.27) obtained at 1450 °C were in agreement with each other, which also indicated that the intrinsic factor of ionic polarizability played a predominant role in affecting the properties for the well sintered samples, and the minor deviation from the $\alpha_{theo.}$ and $\alpha_{obs.}$ also indicated that the evaporation of lithium could be neglected in this work.

As shown in Fig. 5, the quality factors of $Li_4Mg_3Ti_2O_9$ steadily increased from 93,000 to 133,500 GHz with the sintering temperature increasing from 1350 to 1425 °C and reached to a maximum value of 135,800 GHz at 1450 °C. The obvious increase of Q·f values from 1350 to 1450 °C was also attributed to the decreased porosity and increased grain sizes shown in Figs. 1 and 2. It was well known that density took little effect on Q·f values for the sintered well samples, while crystal structure and phase composition played an important role in affecting dielectric loss at higher sintering temperature [1,2]. Fig. 5 also illustrated the temperature coefficient of resonant frequency of $Li_4Mg_3Ti_2O_9$ as a function of the sintering temperature. Before the τ_f values fluctuating from −7.06 to −9.13 ppm/°C in the temperature

Table 1
Bond types, bond length, bond ionicity and lattice energy of $Li_4Mg_3Ti_2O_9$ sintered at 1450 °C.

Bond Type	Bond length (Å)	C^{μ} (eV)	E_h^{μ} (eV)	E_g^{μ} (eV)	$\exp(-k_s^{\mu}r_0^{\mu})$	f_i^{μ}	f_c^{μ}	U_{bc} (kJ/mol)	U_{bi} (kJ/mol)	U (kJ/mol)
Li-O	2.0816	−11.0514	6.4506	12.7963	0.0499	0.7460	0.2540	103	368	471
Mg-O	2.0816	−15.3099	6.4506	16.6134	0.0345	0.8493	0.1507	190	1674	1864
Ti-O	2.0816	−20.2768	6.4506	21.2781	0.0229	0.9082	0.0918	360	7162	7522

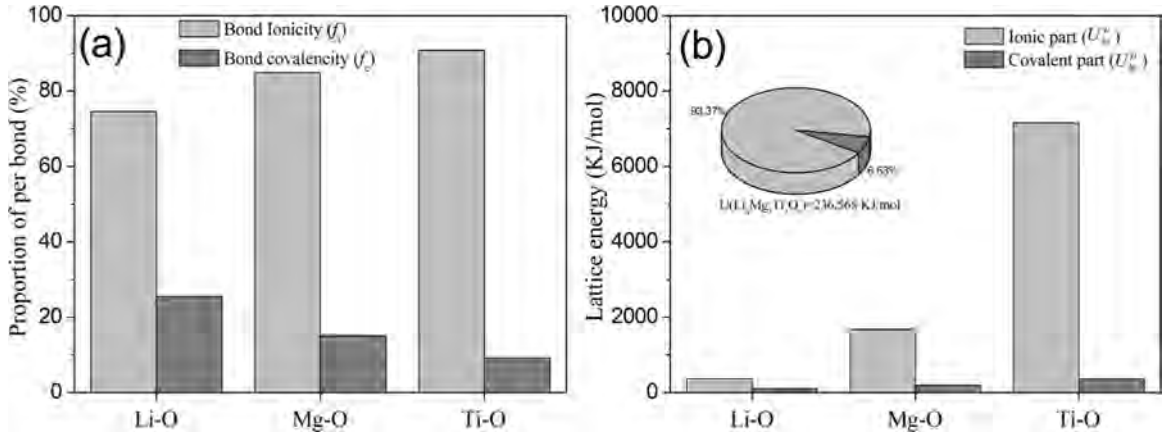

Fig. 4. Bond ionicity and lattice energy of $Li_4Mg_3Ti_2O_9$ ceramics sintered at 1450 °C.

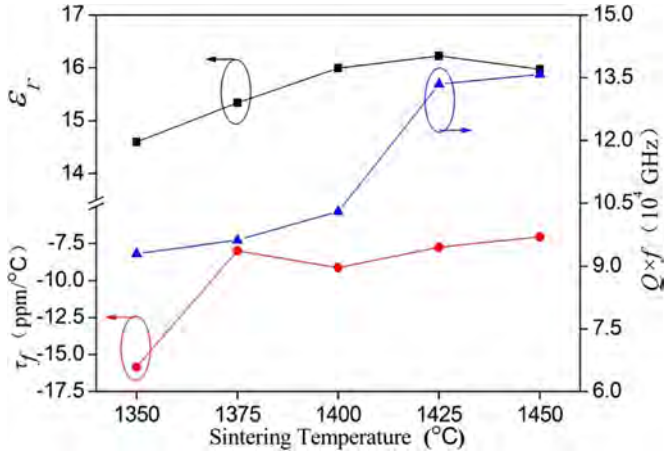

Fig. 5. ε_r, $Q{\cdot}f$ and τ_f values of $Li_4Mg_3Ti_2O_9$ ceramics as a function of sintering temperatures from 1350 to 1450 °C.

region of 1375–1450 °C, there was a significant growth below 1375 °C, which might be caused by the variation of apparent density. The excellent dielectric properties of $Li_4Mg_3Ti_2O_9$ could be obtained at 1450 °C with ε_r=15.97, $Q{\cdot}f$ =135,800 GHz and τ_f=−7.06 ppm/°C. By comparison, the Li_2MgTiO_4 synthesized by the same method possessed a lower $Q{\cdot}f$ of 97,629 GHz combined with ε_r=15.07 and τ_f=−3.81 ppm/°C [15], while the properties of $Li_2Mg_3TiO_6$ were ε_r=14.42, $Q{\cdot}f$=153,000 GHz and τ_f=−11.07 ppm/°C [16]. Hence, it could be concluded that $Li_4Mg_3Ti_2O_9$ possessed the excellent performance in the Li_2TiO_3-MgO system.

The measured and calculated IR reflectivity spectra of the $Li_4Mg_3Ti_2O_9$ ceramics sintered at 1450 °C were illustrated in Fig. 6(a). According to the classical oscillator model, the complex dielectric function was written as Eq. (13), and the fitted data could be obtained by Fresnel formula shown in Eq. (14) [29–32].

$$\varepsilon^*(\omega) = \varepsilon_\infty + \sum_{j=1}^{n} \frac{S_j}{\omega_j^2 - \omega^2 + i\omega\gamma_j} \tag{13}$$

$$R = \left| \frac{\sqrt{\varepsilon^*} - 1}{\sqrt{\varepsilon^*} + 1} \right|^2 \tag{14}$$

where $\varepsilon^*(\omega)$ was the complex dielectric function, R(ω) was the IR reflectivity, n was the transverse phonon modes number, ε_∞ was the dielectric constant affected by electronic polarization in higher frequencies, S_j, ω_j and γ_j were the intensity, resonant frequency and coefficient of damping of individual mode, while the lower resonant frequency of specimen [$\omega(\sim 10^9) \ll \omega_j(\sim 10^{12})$] could be neglected in calculating ε'. The reflectivity spectrum of $Li_4Mg_3Ti_2O_9$ was fitted by 5 resonant modes and the calculated IR reflectivity spectrum agreed well with the measured one as observed in Fig. 5(a) and Table 3. In addition, the dielectric loss tangent (tanδ) could be calculated as following Eq. (15).

$$\tan\delta = \frac{\varepsilon''}{\varepsilon'} = \frac{\sum_j \Delta\varepsilon_j'(\gamma_j\omega)/\omega_j^2}{\varepsilon_\infty + \sum_j \Delta\varepsilon_j'(\omega)} \tag{15}$$

$$\varepsilon'' = \sum_{j=1}^{n} \frac{S_j\gamma_j}{\omega_j^2}\omega \tag{16}$$

The measured complex dielectric constants (ε' and ε'') and imaginary function obtained by K-K analysis were shown in Fig. 6(b). The measured ε' (15.97) was higher than the calculated one (10.84) at 10.64 GHz, while the calculated dielectric loss (tanθ=0.0000750) was equal to the measured value (tanθ=1/Q=0.000608). Hence, it could be deduced that the absorptions of phonon oscillation at infrared frequency played a major role in contributing the polarization of $Li_4Mg_3Ti_2O_9$.

The XRD patterns of $Li_4Mg_3Ti_2O_9$ ceramics doped with different amounts of LiF sintered at 900 °C were shown in Fig. 7. As shown in the standard card of JCPDS #70-1934, the cubic rock salt structured LiF possessed appropriate lattice parameters of a=b=c=4.026 Å and V=65.30 Å^3, which were close to that of $Li_4Mg_3Ti_2O_9$ ceramics sintered at 1450 °C (V=72.12 Å^3 with a=b=c=4.1626 Å). The above sintering aid had a low melting point less than 900 °C, which could significantly

Table 2
Lattice parameters, microwave dielectric properties, theoretical dielectric polarizability ($\alpha_{theo.}$) and observed dielectric polarizability ($\alpha_{obs.}$) of $Li_4Mg_3Ti_2O_9$ ceramics sintered from 1350 to 1450 °C.

Sintering Temperature (°C)	V_m (Å^3)	a=b=c (Å)	ε_r	$\alpha_{theo.}$	$\alpha_{obs.}$	$Q{\cdot}f$ (×10^4 GHz)	τ_f (ppm/°C)
1350	72.22	4.1643	15.60	32.17	32.18	9.30	−15.86
1375	72.18	4.1636	15.34	32.17	32.06	9.62	−7.99
1400	72.16	4.1633	15.99	32.17	32.30	10.30	−9.13
1425	72.15	4.1631	16.22	32.17	32.38	13.35	−7.76
1450	72.12	4.1626	15.97	32.17	32.27	13.58	−7.06

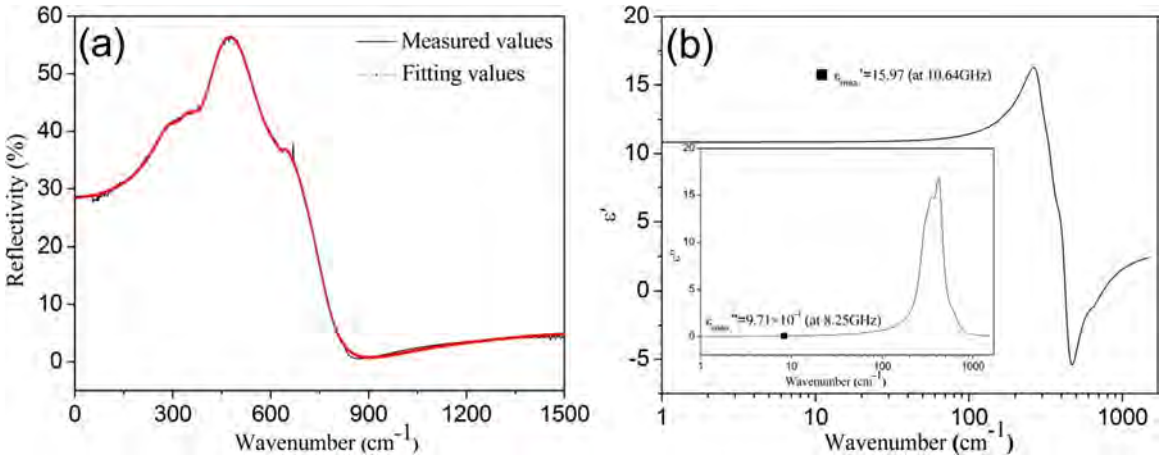

Fig. 6. (a) Measured and fitted IR reflectivity spectrum of $Li_4Mg_3Ti_2O_9$ ceramic sintered at 1450 °C (b) The real and imaginary parts of complex permittivity of $Li_4Mg_3Ti_2O_9$ ceramic sintered at 1450 °C. (For interpretation of the references to color in this figure legend, the reader is referred to the web version of this article.)

Table 3
Fitted parameters of resonant modes in $Li_4Mg_3Ti_2O_9$ ceramics sintered at 1450 °C.

Mode	$Li_4Mg_3Ti_2O_9$ ε_∞=3.04			
	ω_{oj}	ω_{pj}	γ_j	$\Delta_{\varepsilon j}$
1	294.62	394.45	83.346	1.79000
2	348.34	504.63	93.620	2.10000
3	426.54	792.72	107.300	3.45000
4	604.53	409.05	204.550	0.45800
5	638.44	49.35	30.823	0.00598

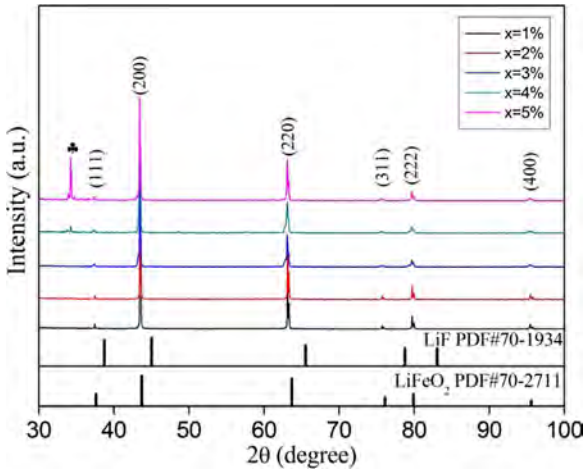

Fig. 7. XRD patterns of $Li_4Mg_3Ti_2O_9$-x wt% LiF ceramics sintered at 900 °C for 4 h.

enhance the formation of $Li_4Mg_3Ti_2O_9$ at lower sintering temperatures. As shown in Fig. 7, it could be observed that the only rock-salt structured $Li_4Mg_3Ti_2O_9$ phase appeared in the XRD patterns of the specimens with less than 3 wt% LiF additions. Hence, it could be considered that the continuous solid solutions between $Li_4Mg_3Ti_2O_9$ and LiF were formed in this work. What's more, the similar results were also confirmed in other Li_2O-MgO-TiO_2 + LiF systems [17,18]. However, abnormal diffraction peak was observed at around 34° when the specimens were doped with 4–5 wt% LiF, which could not match the standard cards of $Li_4Mg_3Ti_2O_9$ and LiF. It might be considered that the large amount of liquid phase would result in the formation of non-stoichiometric compounds and excessive oxygen vacancies.

Fig. 8 illustrated the variation in the apparent densities of $Li_4Mg_3Ti_2O_9$-x wt% LiF (x=1–5) as a function of sintering temperature. When the samples were added with 1–2 wt% LiF, the apparent

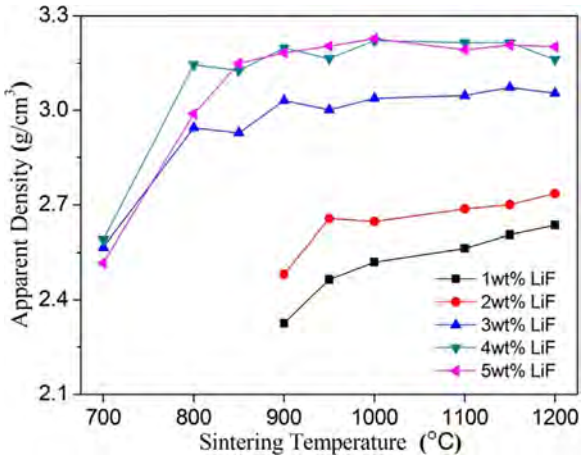

Fig. 8. Curves of apparent densities of $Li_4Mg_3Ti_2O_9$-x wt% LiF ceramics sintered for 4 h depending on sintering temperatures from 700 to 1200 °C.

densities gradually increased with the temperature increasing from 900 to 1200 °C. The relatively high values of these samples could be obtained at 1200 °C (2.64 g/cm^3 for x=1, 2.74 g/cm^3 for x=2). The apparent density of $Li_4Mg_3Ti_2O_9$-3 wt% LiF ceramics reached to 3.03 g/cm^3 at 900 °C, which was close to that of matrix (3.15 g/cm^3) obtained at 1425–1450 °C for 4 h. Hence, it could be considered that the addition of LiF was one of the effective methods to decrease the sintering temperatures of $Li_4Mg_3Ti_2O_9$ system. Similarly, samples with 4 wt% and 5 wt% LiF additions obtained their maximum densities of 3.20 g/cm^3 at 900 °C, which was mainly due to the reduced porosity caused by excessive liquid phase. Thus, it could be concluded that there were no significant changes of apparent densities in the temperature region of 900–1200 °C for the specimens with 3–5 wt% LiF.

To clarify the microstructure of LiF-doped $Li_4Mg_3Ti_2O_9$ ceramics, the scanning electron micrographs of x wt% LiF doped specimens (sintered at 900 °C) were shown in Fig. 9. Large amounts of small grains and pores could be observed in the surface of samples with 1–2 wt% LiF addition, implying that the grain growth was incomplete due to the small amount of liquid phase. By contrast, the porosity of $Li_4Mg_3Ti_2O_9$-3 wt% LiF ceramics decreased significantly with an average grain size of about 3 μm, and similarly no visible microspores and cracks could be detected for the $Li_4Mg_3Ti_2O_9$ samples doped with 4–5 wt% LiF. Although the average grain sizes of LiF doped $Li_4Mg_3Ti_2O_9$ ceramics were much less than those of matrix sintered above 1350 °C, the addition of LiF remarkably improved the sintering characteristics of $Li_4Mg_3Ti_2O_9$ ceramics. Additionally, there were different shapes of grains in Fig. 9(e), which was consistent with

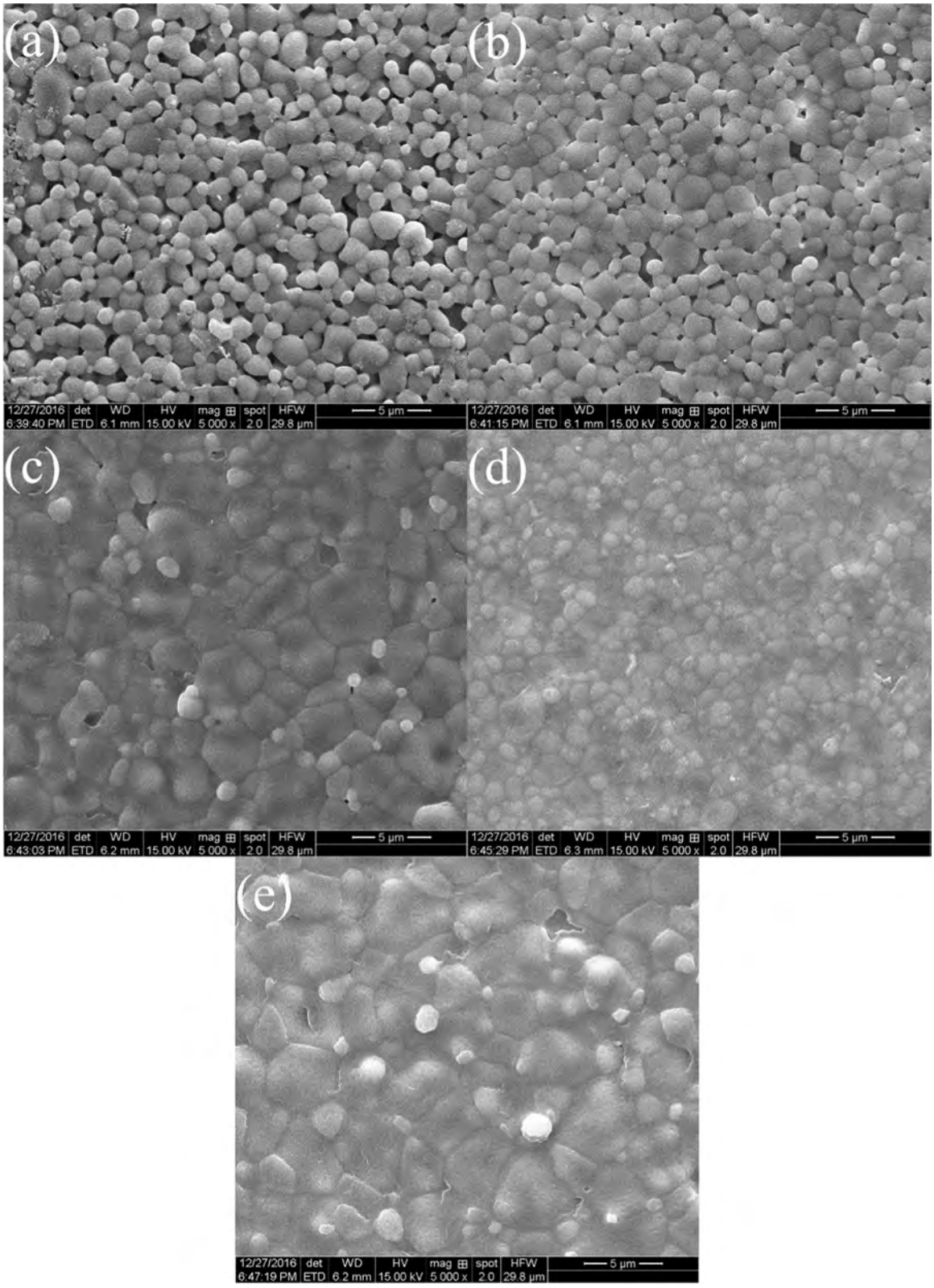

Fig. 9. SEM micrographs of $Li_4Mg_3Ti_2O_9$-x wt% LiF ceramics sintered at 900 °C for 4 h (a-e corresponding to x=1, x=2, x=3, x=4, and x=5).

results of XRD patterns shown in Fig. 7.

Fig. 10 demonstrated the variation of microwave dielectric properties of $Li_4Mg_3Ti_2O_9$-x wt% LiF ceramics. As shown in Fig. 10(a) and (c), the variation in dielectric constants with sintering temperature were consistent with that of apparent densities, which suggested the porosity of ceramics was the dominating extrinsic factor to control ε_r values. For the specimens with 3–5 wt% LiF, the saturated ε_r values could be obtained at 900 °C with a sequence of $\varepsilon_{r(x=5\ wt\%)} > \varepsilon_{r(x=4\ wt\%)} > \varepsilon_{r(x=3\ wt\%)}$. The above results could be explained in terms of both increased relative densities and additional polarizabilities of Li^+ and F^- ions.

As shown in Fig. 10(b), an increasing trend could be witnessed in the $Q{\cdot}f$ values with the increasing sintering temperature. For instance,

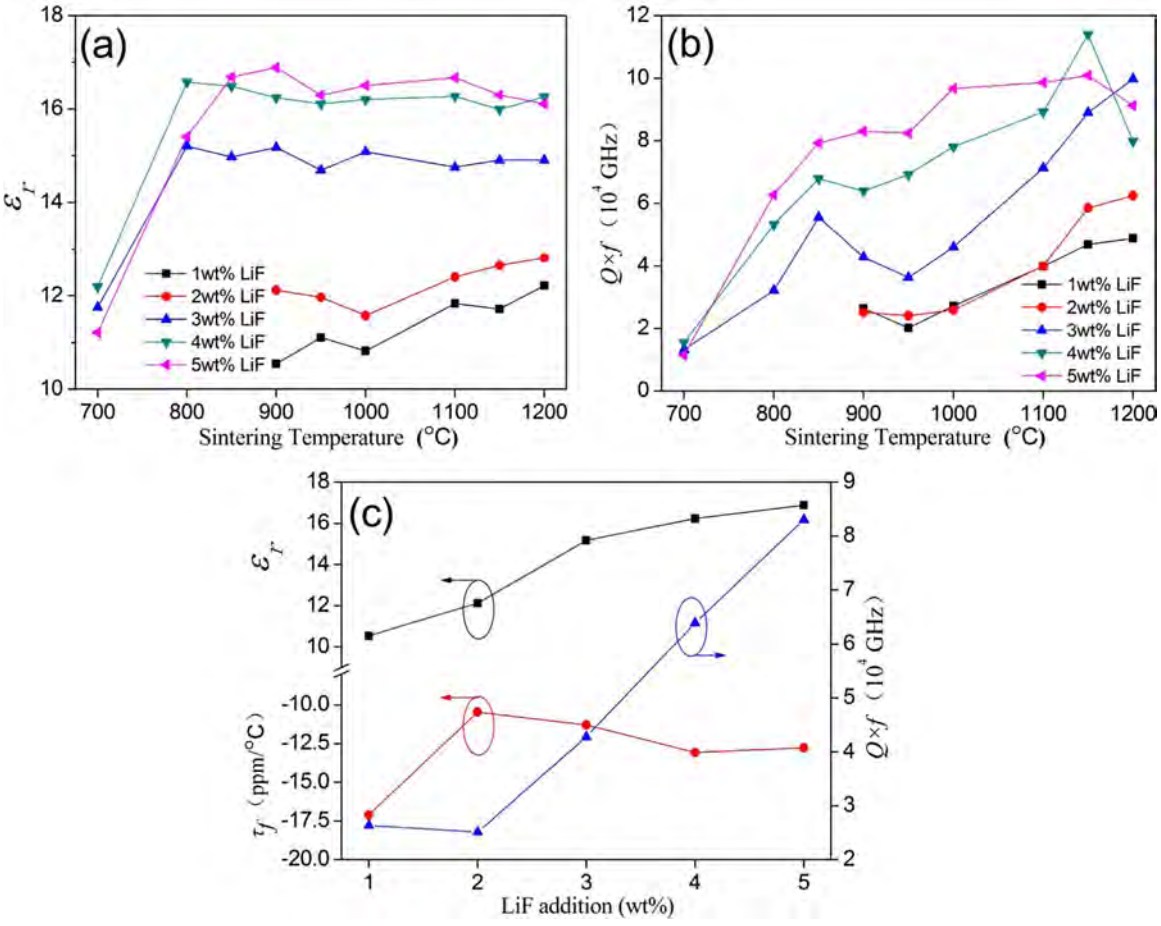

Fig. 10. Curves of (a) dielectric constants and (b) quality factors of $Li_4Mg_3Ti_2O_9$-x wt% LiF ceramics sintered for 4 h depending on sintering temperatures from 700 to 1200 °C, (c) Curves of ε_r, $Q{\cdot}f$ and τ_f values of $Li_4Mg_3Ti_2O_9$-x wt% LiF ceramics sintered at 900 °C.

the $Q{\cdot}f$ values of 1 wt% LiF-doped $Li_4Mg_3Ti_2O_9$ ceramics increased from 26,400 GHz at 700 °C to 46,800 GHz at 1200 °C, which was correlated with the increasing apparent densities shown in Fig. 8. However, for the samples with 3 wt% LiF, the $Q{\cdot}f$ values significantly increased from 13,200 to 99,800 GHz with the temperature increasing from 700 to 1200 °C. Although the specimens got densified at 900 °C, the grain sizes seemed to play a predominant role in affecting the dielectric loss. There was the maximum quality factor of 114,000 GHz at 1150 °C for $Li_4Mg_3Ti_2O_9$-4 wt% LiF ceramic, which was similar with the values obtained by the matrix. In addition, for those specimens sintered at 900 °C, the $Q{\cdot}f$ values increased with the addition of LiF as shown in Fig. 10(c).

The τ_f values of $Li_4Mg_3Ti_2O_9$-x wt% LiF ceramics sintered at 900 °C were also shown in Fig. 10(c). With the additions of LiF increasing from 1 to 2 wt%, the τ_f values increased from −17.12 to −10.46 ppm/°C, implying that the temperature stability of ceramics was sensitive to the apparent densities. After that, the values fluctuated around −10 ppm/°C with the increase of LiF content from 3 to 5 wt%. Typically, the $Li_4Mg_3Ti_2O_9$-3 wt% LiF ceramics possessed a single phase with an appropriate microwave dielectric property of ε_r=15.17, $Q{\cdot}f$ =42,800 GHz and τ_f=−11.30 ppm/°C, which made the samples suitable for the LTCC application.

4. Conclusion

The novel rock-salt structured $Li_4Mg_3Ti_2O_9$ ceramics were successfully prepared by the conventional solid-state method. The relationship among phase composition, sintering characteristics, bond characteristics, infrared spectra and microwave dielectric properties was firstly investigated. The excellent dielectric properties of $Li_4Mg_3Ti_2O_9$ could be obtained at 1450 °C with ε_r=15.97, $Q{\cdot}f$ =135,800 GHz and τ_f=−7.06 ppm/°C. The extrapolated permittivity and dielectric loss obtained from fitted reflectivity spectra matched well with the measured values, which indicated that the polar optical phonons played a dominated role in affecting polarization behavior. The addition of LiF could effectively improve the sintering characteristics of matrix. The $Li_4Mg_3Ti_2O_9$-3 wt% LiF ceramics sintered at 900 °C exhibited the single phase with the properties of ε_r=15.17, $Q{\cdot}f$ =42,800 GHz and τ_f=−11.30 ppm/°C.

Acknowledgments

This work was supported by the National Natural Science Foundation (No. 51472108) and National Training Plan Innovation Project of college students (No. 201610427016). The authors are thankful to the administrators in IR beamline workstation of National Synchrotron Radiation Laboratory (NSRL) for the help in IR measurement. The authors are thankful to the help of Professor ZhenXing Yue and postdoctoral Jie Zhang on the measurement of microwave properties in Tsinghua University.

References

[1] M.T. Sebastian, Dielectric Materials for Wireless Communication, Elsevier, Oxford, 2008.
[2] A. Terrell, Vanderah, Talking ceramics, Science 298 (2002) 1182–1184.
[3] H. Ohsato, Functional advances of microwave dielectrics for next generation, Ceram. Int. 38 (2012) S141–S146.
[4] R.J. Cava, Dielectric materials for applications in microwave communications, J. Mater. Chem. 11 (2001) 54–62.

[5] I.M. Reaney, D. Iddles, Microwave dielectric ceramics for resonators and filters in mobile phone networks, J. Am. Ceram. Soc. 89 (2006) 2063–2072.
[6] M.T. Sebastian, H. Jantunen, Low loss dielectric materials for LTCC applications: a review, Int. Mater. Rev. 53 (2008) 57–90.
[7] S. George, M.T. Sebastian, Synthesis and microwave dielectric properties of novel temperature stable high Q, $Li_2ATi_3O_8$ (A=Mg, Zn) ceramics, J. Am. Ceram. Soc. 93 (2010) 2164–2166.
[8] H.F. Zhou, X.B. Liu, X.L. Chen, L. Fang, Preparation, phase structure and microwave dielectric properties of a new low cost $MgLi_{2/3}Ti_{4/3}O_4$ compound, Mater. Chem. Phys. 137 (2012) 22–25.
[9] Y.D. Zhang, D. Zhou, Pseudo phase diagram and microwave dielectric properties of Li_2O-MgO-TiO_2 ternary system, J. Am. Ceram. Soc. 99 (2016) 3645–3650.
[10] M. Castellanos, A.R. West, Order-disorder phenomena in oxides with rock salt structures: the system Li_2TiO-MgO, J. Mater. Sci. 14 (1979) 450–454.
[11] J.J. Bian, Y.F. Dong, New high Q microwave dielectric ceramics with rock salt structures: (1-x)li_2TiO_3-xMgO system (0≤x≤0.5), J. Eur. Ceram. Soc. 2 (2010) 325–330.
[12] Z.F. Fu, P. Liu, J.L. Ma, X.G. Zhao, H.W. Zhang, Novel series of ultra-low loss microwave dielectric ceramics: $Li_2Mg_3BO_6$ (B = Ti, Sn, Zr), J. Eur. Ceram. Soc. 3 (2016) 625–629.
[13] Y.W. Tseng, J.Y. Chen, Y.C. Kuo, C.L. Huang, Low-loss microwave dielectrics using rock salt oxide Li_2MgTiO_4, J. Alloy. Compd. 509 (2015) L308–L310.
[14] H.F. Zhou, X.H. Tan, J. Huang, N. Wang, G.H. Fan, X.L. Chen, Phase structure, sintering behavior and adjustable microwave dielectric properties of $Mg_{1-x}Li_{2x}Ti_xO_{1+2x}$ solid solution ceramics, J. Alloy. Compd. 696 (2017) 1255–1259.
[15] H.L. Pan, C.F. Xing, X.S. Jiang, H.T. Wu, Characterization on low loss dielectric Li_2MgTiO_4 ceramics based on chemical bond theory at microwave frequency, J. Alloy. Compd. 688 (2016) 416–421.
[16] H.T. Wu, E.S. Kim, Correlations between crystal structure and dielectric properties of high-Q materials in rock-salt structure Li_2O-MgO-BO_2 (B=Ti, Sn, Zr) systems at microwave frequency, RSC Adv. 6 (2016) 47443–47453.
[17] Z.F. Fu, P. Liu, J.L. Ma, X.M. Chen, H.W. Zhang, New high Q low-fired $Li_2Mg_3TiO_6$ microwave dielectric ceramics with rock salt structure, Mater. Lett. 164 (2016) 436–439.
[18] Y.Z. Hao, H. Yang, G.H. Chen, Q.L. Zhang, Microwave dielectric properties of Li_2TiO_3 ceramics doped with LiF for LTCC applications, J. Alloy. Compd. 552 (2013) 173–179.
[19] B.W. Hakki, P.D. Coleman, A dielectric resonator method of measuring inductive capacities in the millimeter range, IRE Trans. Microw. Theory Tech. 8 (1960) 402–410.
[20] W.E. Courtney, Analysis and evaluation of a method of measuring the complex permittivity and permeability of microwave insulators, IEEE Trans. Microw. Theory Tech. 18 (1970) 476–485.
[21] D.F. Xue, S.Y. Zhang, Calculation of the nonlinear optical coefficient of the $NdAl_3(BO_3)_4$ crystal, J. Phys.: Condens. Matter 8 (1996) 1949–1956.
[22] Z.J. Wu, Q.B. Meng, S.Y. Zhang, Semi empirical study on the valences of Cu and bond covalency in $Y_{1-x}Ca_xBa_2Cu_3O_{6+y}$, Phys. Rev. B 58 (1998) 958–962.
[23] Q.B. Meng, Z.J. Wu, S.Y. Zhang, Evaluation of the energy barrier distribution in many-particle systems using the path integral approach, Phys. Condens. Matter 10 (1998) 85–88.
[24] B.F. Levine, Bond susceptibilities and ionicities in complex crystal structures, J. Chem. Phys. 59 (1973) 1463–1486.
[25] S.S. Batsanov, Dielectric methods of studying the chemical bond and the concept of electronegativity, Russ. Chem. Rev. 51 (1982) 684–697.
[26] M. Birkholz, The crystal energy of pyrite, J. Phys.: Condens. Matter. 4 (1992) 6227–6240.
[27] R.D. Shannon, G.R. Rossman, Dielectric constants of silicate garnets and the oxide additivity rule, Am. Miner. 77 (1992) 94–100.
[28] R.D. Shannon, Dielectric polarizabilities of ions in oxides and fluorides, J. Appl. Phys. 73 (1993) 348–366.
[29] J. Petzelt, S. Kamba, Submillimetre and infrared response of microwave materials: extrapolation to microwave properties, Mater. Chem. Phys. 79 (2003) 175–180.
[30] K.P.F. Siqueira, R.L. Moreira, A. Dias, Synthesis and crystal structure of lanthanide orthoniobates studied by vibrational spectroscopy, Chem. Mater. 22 (2010) 2668–2674.
[31] L.X. Pang, D. Zhou, J. Guo, Z.M. Qi, T. Shao, Microwave dielectric properties of scheelite structured low temperature fired $Bi(In_{1/3}Mo_{2/3})O_4$ ceramic, Ceram. Int. 39 (2013) 4719–4722.
[32] E.S. Kim, W. Choi, Effect of phase transition on the microwave dielectric properties of $BiNbO_4$, J. Eur. Ceram. Soc. 26 (2006) 1761–1766.